



Investigation of structural, electrical and optical properties of $\text{SnS}_{0.75}\text{Se}_{0.25}$ ternary alloy crystals

Vibhuti P. Jethwa^{1,*} , Kunjal Patel¹, Vivek M. Pathak¹, and Gunvant K. Solanki¹

¹Department of Physics, Sardar Patel University, Vallabh Vidyanagar, Gujarat 388120, India

Received: 31 March 2021

Accepted: 5 August 2021

Published online:

11 August 2021

© The Author(s), under exclusive licence to Springer Science+Business Media, LLC, part of Springer Nature 2021

ABSTRACT

The crystals of ternary-mixed compounds of group IV–VI have been grown using the direct vapour transport technique. The grown crystals of $\text{SnS}_{0.75}\text{Se}_{0.25}$ were characterized to investigate the compositional, structural, electrical and optical properties using appropriate techniques. The composition analysis confirms the stoichiometric proportion of Sn, S and Se. The structural analysis of the grown crystals reveals their layered-type growth mechanism and crystallinity of grown materials. The selected area electron diffraction patterns were also recorded from nanocrystals using e-beams. The formation of $\text{SnS}_{0.75}\text{Se}_{0.25}$ ternary alloy was confirmed by X-ray photoelectron spectroscopy. The temperature-dependent electrical resistivity measurement was performed to study the anisotropy of grown layered ternary alloy. From optical absorption spectra, the optical bandgap of the sample was determined. The obtained results were discussed to assess the suitability of the $\text{SnS}_{0.75}\text{Se}_{0.25}$ crystal for the fabrication of optoelectronic devices.

1 Introduction

The semiconducting materials from the IV–VI group have been drawing intense attention due to their potential application in optoelectronic and photovoltaic devices [1–7]. In recent years, among common semiconductors from the IV–VI group, chemically stable and earth-abundant tin chalcogenides have appeared as excellent candidates for great performance photodetector [8, 9]. Tin sulphide and tin selenium exhibit an anisotropic layered orthorhombic structure with an indirect bandgap in the range of 1.0–1.1 eV [10, 11]. Furthermore, they possess an

optimum bandgap for solar cell and high absorption coefficient from ultraviolet (UV) to near-infrared (NIR) was found in the aforementioned materials, making them the leading candidate to be used in the optoelectronic device [12–17]. It has been observed from the literature survey that alloy engineering is one of the approaches to improve the electrical and optical behaviour than individual SnS and SnSe. Both of these materials have been well studied, with only a few pieces of evidence on the formation of ternary compound $\text{SnS}_{0.75}\text{Se}_{0.25}$ alloy. It can be achievable to study intermediate properties in between the SnS and SnSe can be expected with Se incorporation in SnS.

Address correspondence to E-mail: jethwavibhuti95@gmail.com

Hence, it is practicable to enhance to optoelectronic and electronic properties of SnS and SnSe by alloying technique. On such a basis, Se incorporated SnS have been reported to improve the electrical and optoelectrical behaviour of the device. Transition metal chalcogenides are layered materials and exhibit unique electronic properties [18]. The atoms within the layer are covalently bonded with each other and individual adjacent layers are bonded by weak van der Waals forces make it easier to cleave [19, 20]. In accordance with the unique structural property of tin chalcogenides, it is possible to use such materials as solid ion batteries, NIR photodetector, anisotropic field effect transistor, photocatalyst, optical switching, gas sensor and as an anode [21–30]. The crystal of $\text{SnS}_{0.75}\text{Se}_{0.25}$ has a layered mechanism with each layer consisting of Sn–S–Se elements. The intralayer strong bonding and interlayer weak van der Waals bonding gives anisotropic electrical, structural and optical properties [31]. This anisotropic behaviour of transition metal chalcogenides plays an important role in device applications.

This study explores the effect of Se incorporation in SnS and its anisotropic behaviour. The direct vapour transport (DVT) technique is used for the growth of $\text{SnS}_{0.75}\text{Se}_{0.25}$ crystals. The synthesized crystals were characterized by energy dispersive analysis of X-rays (EDAX), scanning electron microscopy (SEM), X-ray diffraction (XRD), high-resolution transmission electron microscopy (HRTEM) and X-ray photoelectron spectroscopy (XPS) to identify chemical compositions, morphology, phases, crystallinity and chemical states, respectively, of the grown crystals. The electrical and optical properties of $\text{SnS}_{0.75}\text{Se}_{0.25}$ crystals were well characterized, to evaluate the activation energy and optical bandgap of synthesized $\text{SnS}_{0.75}\text{Se}_{0.25}$ ternary alloy.

2 Experimental

2.1 Growth of $\text{SnS}_{0.75}\text{Se}_{0.25}$ alloyed crystals

The crystals of multi-layered $\text{SnS}_{0.75}\text{Se}_{0.25}$ were grown by DVT [20]. Primarily the mixture was prepared using highly pure powder of Sn, S and Se, weighted in stoichiometric proportion. The mixture was sealed in a chemically cleaned quartz ampoule under a pressure of 10^{-5} Torr. Then this sealed ampoule was placed in a dual zone horizontal furnace. The furnace

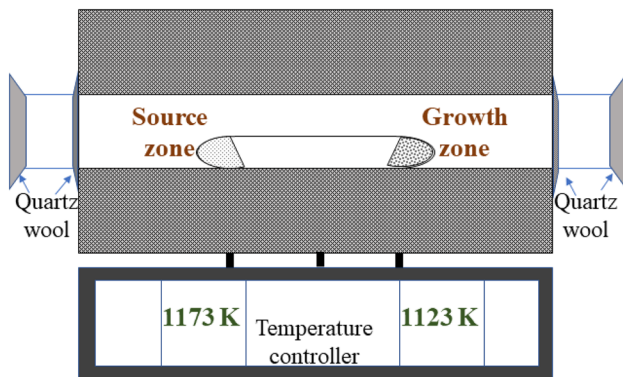
has two zones namely source zone and growth zone. The source zone is one end of ampoule where the mixed powder of the constituent elements is placed and growth zone is the other end of the ampoule where the actual crystal growth takes place. The source zone temperature is generally kept at higher temperature compared to growth zone and a constant temperature gradient of 50 K is maintained throughout the growth process. The temperature of the source zone and growth zone was increased up to 1173 and 1123 K, respectively, with the rate of 26 K/h. The temperature of both the zones were maintained at this temperature for 40 h. At these temperatures, the constituent elements in the form of vapour reacts and gets transported from source zone to growth zone. The total period of growth process is 130 h. Then the temperature of both the zones are cooled to room temperature. During the temperature of the zone reduces, the transported vapour settles down at growth zone forming small and large size crystals, compounds as well as ingots. The resulting crystals along with ingots were collected after breaking the ampoule carefully. The crystal growth parameters are mentioned in Table 1. The schematic diagram for the DVT technique is shown in Fig. 1.

2.2 Characterization

The crystals of $\text{SnS}_{0.75}\text{Se}_{0.25}$ were first characterized by EDAX using EDAX, Philips FE-SEM XL-30 for determination of the proportion of Sn, S and Se in the grown crystal. The surface morphology was examined using SEM using Field Emission Gun Nano Nova FE-SEM 450. The XRD pattern was recorded via a Bruker Advance D8 X-ray diffractometer having $\text{Cu K}\alpha$ (1.5418 Å) radiation. The structural characterization was carried out by HRTEM (JEM-2010 F from JEOL, 200 KV). For the study of HRTEM, the tiny crystallites are dispersed in acetone and the prepared suspension was sonicated for 3 h. Then this prepared suspension was drop casted on copper grid for analysis. The selected area electron diffraction (SAED) pattern was also recorded. The XPS study was carried out using SPECS surface Nano Analysis GmbH Al $\text{K}\alpha$ (1486.61) X-rays, a 13 kV, 100 W ESCA spectrometer. Temperature-dependent electrical resistivity measurement in-plane and out-of-plane direction were carried out in the temperature range 300–693 K. The optical absorbance was obtained using UV–VIS–NIR absorption spectrometer.

Table 1 Growth parameters of $\text{SnS}_{0.75}\text{Se}_{0.25}$ crystals

Crystal	Source zone temperature (K)	Source zone temperature (K)	Growth period (h)	Dimension (mm^3)	Appearance	Colour
$\text{SnS}_{0.75}\text{Se}_{0.25}$	1173	1123	130	$4 \times 3 \times 1$	Plate	Metallic black

**Fig. 1** Schematic diagram of DVT technique

3 Results and discussion

The EDAX analysis of $\text{SnS}_{0.75}\text{Se}_{0.25}$ ternary alloy formed by the DVT technique indicated the presence of Sn, S and Se as constituent elements. Figure 2a indicates the EDAX spectra of $\text{SnS}_{0.75}\text{Se}_{0.25}$ ternary alloy. Figure 2c–f represents the elemental mapping of $\text{SnS}_{0.75}\text{Se}_{0.25}$ crystal and it shows in Fig. 2f the homogeneous elemental distribution of Sn, S and Se. The weight% and atomic percentage of all the elements present in the synthesized compound was determined by EDAX and Elemental Mapping are tabulated in Table 2. The EDAX analysis result confirmed that the stoichiometry of the synthesized ternary alloy $\text{SnS}_{0.75}\text{Se}_{0.25}$ crystal has maintained. The surface morphology by SEM of $\text{SnS}_{0.75}\text{Se}_{0.25}$ crystal by SEM is shown in Fig. 3a, b with a different resolution of 30 and 10 μm , respectively. These images clearly indicate a layer type mechanism of grown ternary alloy crystal.

The XRD pattern of grown ternary alloy $\text{SnS}_{0.75}\text{Se}_{0.25}$ crystal is shown in Fig. 2b, which indicates the crystalline nature of grown crystals. Each presented plane is closely compared with the planes of $\text{SnS}_{0.5}\text{Se}_{0.5}$ (JCPDS Card No. 48-1225) with a small shift in the peak positions because of the change in the proportion of the constituent elements. The intense peak at $2\theta = 31.79^\circ$ corresponding to (400) crystallographic

plane of orthorhombic grown $\text{SnS}_{0.75}\text{Se}_{0.25}$ ternary alloy has been observed. The lattice constants of the grown crystal are $a = 11.350 \text{ \AA}$, $b = 3.998 \text{ \AA}$ and $c = 4.450 \text{ \AA}$, which agrees with the previous report [10, 32, 33]. The unit cell volume and c/a ratio found to be about 201.93 \AA^3 and 0.39, respectively.

HRTEM analysis was performed to confirm the crystallinities of the grown ternary alloy crystals. Figure 3c–e presents the HRTEM images of $\text{SnS}_{0.75}\text{Se}_{0.25}$ nanosheets at different length scale. The HRTEM in Fig. 3d, e shows Moiré fringes as a result of the overlapping of multiple $\text{SnS}_{0.75}\text{Se}_{0.25}$ layers. The Moiré fringes of high-quality HRTEM image with an interplanar distance of 0.28 nm is determined from quantitative Fast-Fourier-Transformed analysis. The obtained interplanar distance is corresponding to (400) reflection peak, which observed as a highly intense peak in the XRD pattern. The SAED pattern is shown in Fig. 3f and it confirms the single crystallinity of the alloyed nanosheets, which belong to the orthorhombic crystal structure.

XPS was performed to analyse chemical states and to confirm the formation of the prepared $\text{SnS}_{0.75}\text{Se}_{0.25}$ ternary alloys. Figure 4 shows the obtained core level peak region spectra of the synthesized material. Figure 4a indicates the doublet peaks of Sn 3d at 487.2 eV and 495.5 eV are corresponding to $3d_{5/2}$ and $3d_{3/2}$, respectively, which is attributed to Sn^{+4} oxidation state [34]. The peak at 162.3 eV corresponding to S^{-2} 2p state depicted in Fig. 4b. The peaks at 54.3 eV and 55.4 eV correspond to Se $3d_{5/2}$ and Se $3d_{3/2}$, which is associated to Se^{-2} oxidation state.

The variation in resistance as a function of temperature within in-plane and out-of-plane is portrayed in Fig. 5a. The downturn in resistance with an increase of temperature in the range 303–693 K indicates the semiconducting nature of grown $\text{SnS}_{0.75}\text{Se}_{0.25}$ ternary alloys. In general, for semiconducting material the temperature-dependent resistivity can be attributed by the Arrhenius Eq. (1):

Fig. 2 **a** EDAX spectra of SnS_{0.75}Se_{0.25} ternary alloy with inset table showing weight and atomic percentage of elements, **b** XRD pattern of SnS_{0.75}Se_{0.25} ternary alloy. Elemental mapping of **c** Sn, **d** S, **e** Se and **f** SnS_{0.75}Se_{0.25} crystal

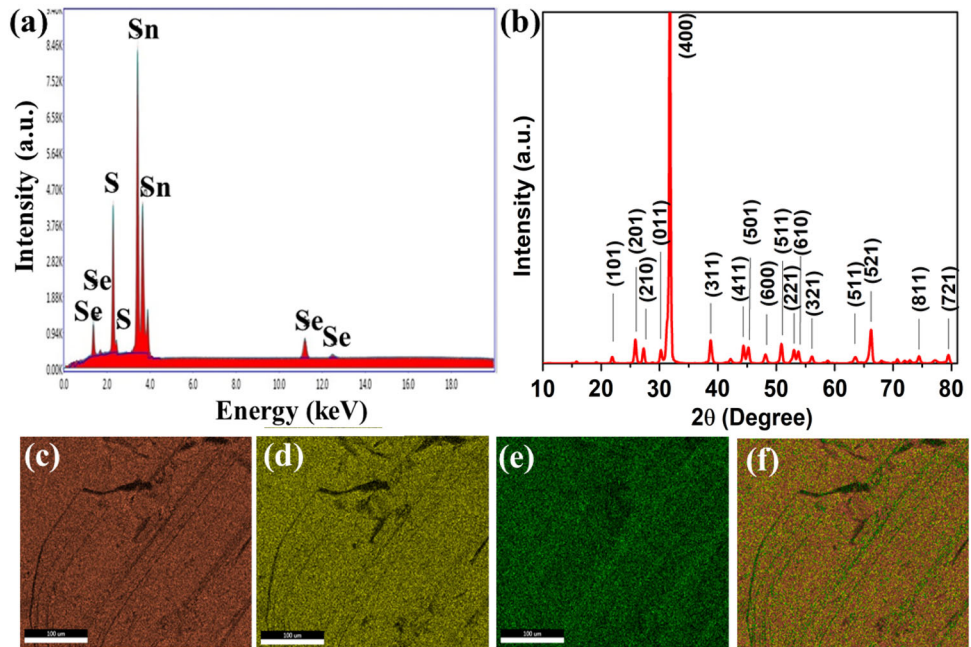
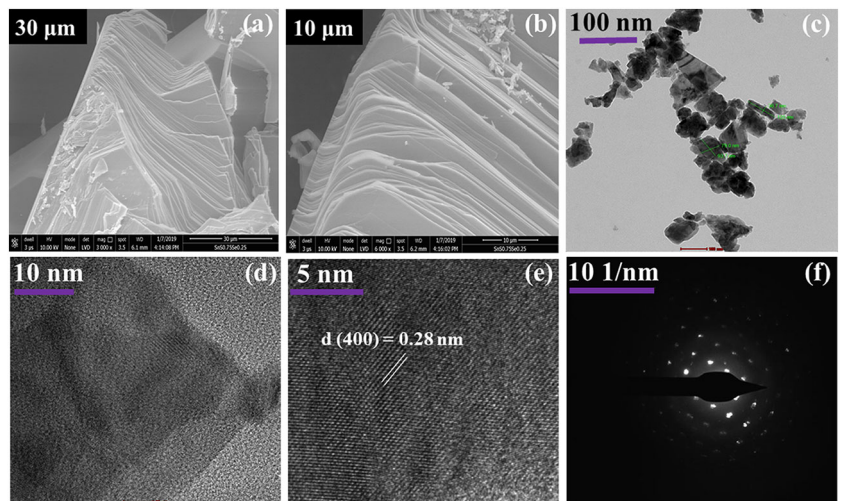


Table 2 Stoichiometric confirmation of grown sample using EDAX and Elemental Mapping analysis with calculated values

Element	Weight (%)			Atomic (%)		
	Calculated for growth	EDAX	Elementalmapping	Calculated for growth	EDAX	Elemental mapping
Sn	73.05	70.14	76.50	50.00	47.44	55.00
S	14.80	14.92	12.40	37.50	37.36	33.00
Se	12.15	14.94	11.10	12.50	15.19	12.00

Fig. 3 **a, b** SEM images of multi-layered SnS_{0.75}Se_{0.25} crystal. HRTEM images of SnS_{0.75}Se_{0.25} crystallites with, **c** length scale of 100 nm, **d** length scale of 10 nm, **e** length scale of 5 nm depicting a d-spacing of 0.28 nm and **f** SAED pattern of SnS_{0.75}Se_{0.25} crystallites

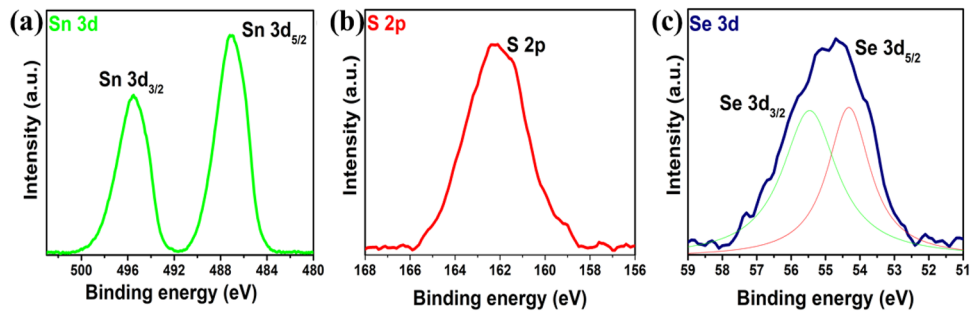


$$\rho = \rho_0 \exp\left(\frac{E_a}{k_b T}\right)$$

(1)

where ρ_0 is the pre-exponential factor, k_b is the Boltzmann constant ($8.6173 \times 10^{-5} \text{ eV K}^{-1}$) and E_a is the activation energy. Figure 5b displays the plot of $\log(\rho)$ versus $1000/T$ of SnS_{0.75}Se_{0.25} crystals, which

Fig. 4 XPS core level region spectra of (a) Sn 3d, (b) S 2p and (c) Se 3d of $\text{SnS}_{0.75}\text{Se}_{0.25}$ ternary alloy



fitted linearly to evaluate the activation energy of the crystals, along the basal plane and perpendicular to the basal plane. The value of activation energy along the basal plane (in-plane) is found to be 0.16 eV and perpendicular to the basal plane (out-of-plane) is found to be 0.19 eV, which can be determined from the slope of the plot ($E_a = 1000 \times \text{slope} \times k_b$). The higher value of activation energy perpendicular to the basal plane suggests the anisotropy in electrical charge conduction in the grown $\text{SnS}_{0.75}\text{Se}_{0.25}$ crystals. The strong interaction along the basal plane and the weak interlayer van der Waals interaction give anisotropic electrical properties. This kind of different interactions results in different inter-atom spacing within in-plane and out-of-plane. Therefore, the electrical transport becomes anisotropic.

The optical response of $\text{SnS}_{0.75}\text{Se}_{0.25}$ ternary thin microcrystallites was characterized by ultraviolet–visible (UV–Vis) spectroscopy. Figure 6a shows the broadband absorption from UV to visible are observed in synthesized ternary nanocrystallites which is in good agreement with reported SnS samples [35, 36], suggesting potential for device applications. The broad absorption spectra closely correspond with a considerable part of the solar radiation spectrum. The optical bandgap of $\text{SnS}_{0.75}\text{Se}_{0.25}$ ternary microcrystallite in N-Methyl-2-

pyrrolidone (NMP) solution is evaluated to be 1.07 eV from the Tauc's plot which is depicted in Fig. 6b.

4 Conclusions

The effect of alloy engineering on the properties of $\text{SnS}_{0.75}\text{Se}_{0.25}$ crystal is presented. We have initially synthesized crystals of $\text{SnS}_{0.75}\text{Se}_{0.25}$ ternary alloy by the DVT technique. EDAX and SEM analysis confirm the elemental compositions and layered-type growth mechanism, respectively. The orthorhombic phase of grown material was studied by the XRD pattern. The chemical states of the grown ternary alloy is confirmed by XPS analysis. The temperature-dependent resistivity measurement in-plane and out-of-plane from room temperature to 693 K were carried out and the activation energy was evaluated. This experiment further confirmed the semiconducting nature of the grown crystals as well as the anisotropic charge conduction mechanism due to layered crystals. The optical properties of grown ternary alloys were investigated by UV–vis spectrophotometer. The optical bandgap of the synthesized alloy is evaluated which came out to be 1.07 eV. This bandgap is well suitable for optoelectronic device applications.

Fig. 5 In-plane and out-of-plane **a** plot of Resistance versus Temperature and **b** plot of $\log(\rho)$ vs. $1000/T$

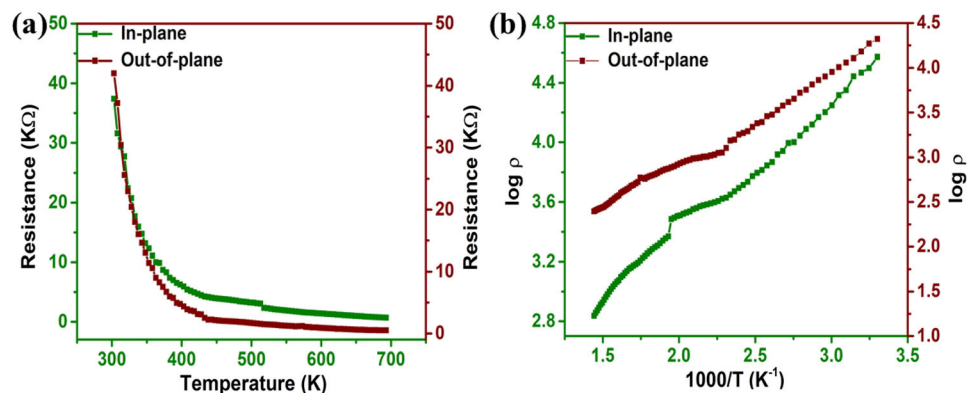
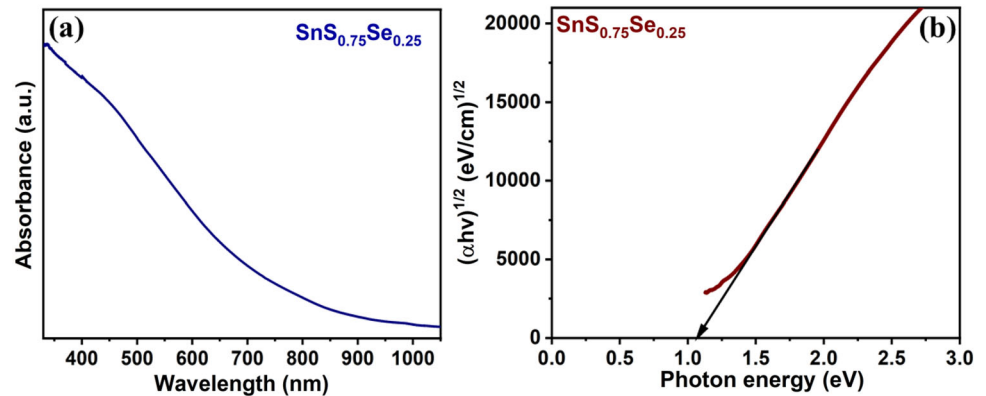


Fig. 6 **a** UV–Vis absorption spectra, **b** Tauc's plot of $(\alpha h\nu)^{1/2}$ as a function of the photon energy of $\text{SnS}_{0.75}\text{Se}_{0.25}$ ternary microcrystallites



Acknowledgements

One of the authors, Miss. Vibhuti P. Jethwa is thankful to the Government of Gujarat for providing financial support under the SHODH funding scheme (Student Ref. No: 201901640012). The author would also like to thank UGC-DAE-Consortium for Scientific Research, Indore for providing the characterization facilities of X-ray Photoelectron Spectroscopy (XPS). The author would also like to thank Dr. Uday Deshpande, UGC-DAE-Consortium for Scientific Research, Indore for the XPS analysis.

Declarations

Conflict of interest There are no conflict of interest to declare.

References

1. P. Pataniya, G.K. Solanki, C.K. Zankat, M. Tannarana, K.D. Patel, V.M. Pathak, *J. Mater. Sci. Mater. Electron.* **30**, 3137 (2019)
2. C.K. Zankat, P. Pataniya, M. Tannarana, G.K. Solanki, K.D. Patel, V.M. Pathak, *J. Mater. Sci. Mater. Electron.* **30**, 6065 (2019)
3. A.J. Khimani, S.H. Chaki, S.M. Chauhan, M.P. Deshpande, *J. Mater. Sci. Mater. Electron.* **30**, 13118 (2019)
4. P. Chauhan, A.B. Patel, K. Patel, A. Patel, G.K. Solanki, K.D. Patel, V.M. Pathak, *J. Mater. Sci. Mater. Electron.* **31**, 11123 (2020)
5. N.F. Patel, S.A. Bhakhar, G.K. Solanki, K.D. Patel, V.M. Pathak, C.K. Zankat, P.M. Pataniya, J.D. Gohil, S.U. Gupta, *J. Mater. Sci. Mater. Electron.* **32**, 11805 (2021)
6. W. Gao, Y. Li, J. Guo, M. Ni, M. Liao, H. Mo, J. Li, *Nanoscale* **10**, 8787 (2018)
7. V.P. Jethwa, K. Patel, V.M. Pathak, G.K. Solanki, *J. Alloys Compd.* **883**, 160941 (2021)
8. P.D. Antunez, J.J. Buckley, R.L. Brutchey, *Nanoscale* **3**, 2399 (2011)
9. R. Zhuo, S. Zuo, W. Quan, D. Yan, B. Geng, J. Wang, X. Men, *RSC Adv.* **8**, 761 (2018)
10. S. Wang, X. Lai, B. Du, J. Ma, P. Wang, J. Jian, *Powder Diff.* **35**, 276 (2020)
11. S.A. Zaki, M.I. Abd-Elrahman, A.A. Abu-Seqhly, N.M. Shaalan, M.M. Hafiz, *Mater. Sci. Semicond. Process.* **75**, 214 (2018)
12. J. Yao, G. Yang, *Nanoscale* **12**, 454 (2020)
13. W.J. Baumgardner, J.J. Choi, Y.F. Lim, T. Hanrath, *J. Am. Chem. Soc.* **132**, 9519 (2010)
14. R. Guo, X. Wang, Y. Kuang, B. Huang, *Phys. Rev. B—Condens. Matter Mater. Phys.* **92**, 1 (2015)
15. A.K. Deb, V. Kumar, *Phys. Status Solidi Basic Res.* **254**, 1 (2017)
16. Y. Huang, L. Li, Y.H. Lin, C.W. Nan, *J. Phys. Chem. C* **121**, 17530 (2017)
17. Y. Wang, L. Huang, B. Li, J. Shang, C. Xia, C. Fan, H.X. Deng, Z. Wei, J. Li, *J. Mater. Chem. C* **5**, 84 (2017)
18. K. Patel, P. Chauhan, A.B. Patel, G.K. Solanki, K.D. Patel, V.M. Pathak, *ACS Appl. Nano Mater.* **3**, 11143 (2020)
19. S.S. Hegde, A.G. Kunjomana, K.A. Chandrasekharan, K. Ramesh, M. Prashantha, *Phys. B Condens. Matter* **406**, 1143 (2011)
20. V.P. Jethwa, K. Patel, N. Som, V.M. Pathak, K.D. Patel, G.K. Solanki, P.K. Jha, *Appl. Surf. Sci.* **531**, 147406 (2020)
21. M. Patel, H.S. Kim, J. Kim, *Nanoscale* **9**, 15804 (2017)
22. J.H. Ahn, M.J. Lee, H. Heo, J.H. Sung, K. Kim, H. Hwang, M.H. Jo, *Nano Lett.* **15**, 3703 (2015)
23. Z. Tian, C. Guo, M. Zhao, R. Li, J. Xue, *ACS Nano* **11**, 2219 (2017)
24. X. Zhou, L. Gan, Q. Zhang, X. Xiong, H. Li, Z. Zhong, J. Han, T. Zhai, *J. Mater. Chem. C* **4**, 2111 (2016)

25. L. Wu, Z. Xie, L. Lu, J. Zhao, Y. Wang, X. Jiang, Y. Ge, F. Zhang, S. Lu, Z. Guo, J. Liu, Y. Xiang, S. Xu, J. Li, D. Fan, H. Zhang, *Adv. Opt. Mater.* **6**, 1 (2018)
26. S. Sucharitakul, U. Rajesh Kumar, R. Sankar, F.C. Chou, Y.T. Chen, C. Wang, C. He, R. He, X.P.A. Gao, *Nanoscale* **8**, 19050 (2016)
27. T. Zhou, W.K. Pang, C. Zhang, J. Yang, Z. Chen, H.K. Liu, Z. Guo, *ACS Nano* **8**, 8323 (2014)
28. M.A. Franzman, C.W. Schlenker, M.E. Thompson, R.L. Brutchey, *J. Am. Chem. Soc.* **132**, 4060 (2010)
29. K.A. Campbell, *Microelectron. J.* **59**, 10 (2017)
30. J. Ning, G. Xiao, T. Jiang, L. Wang, Q. Dai, B. Zou, B. Liu, Y. Wei, G. Chen, G. Zou, *CrystEngComm* **13**, 4161 (2011)
31. M. Patel, J. Kim, Y.K. Kim, *Adv. Funct. Mater.* **28**, 1 (2018)
32. H.S. Im, Y. Myung, K. Park, C.S. Jung, Y.R. Lim, D.M. Jang, J. Park, *RSC Adv.* **4**, 15695 (2014)
33. H. Wei, Y. Su, S. Chen, Y. Lin, Z. Yang, X. Chen, Y. Zhang, *J. Mater. Chem.* **21**, 12605 (2011)
34. D.H. Youn, S.K. Stauffer, P. Xiao, H. Park, Y. Nam, A. Dolocan, G. Henkelman, A. Heller, C.B. Mullins, *ACS Nano* **10**, 10778 (2016)
35. W. Huang, Z. Xie, T. Fan, J. Li, Y. Wang, L. Wu, D. Ma, Z. Li, Y. Ge, Z.N. Huang, X. Dai, Y. Xiang, J. Li, X. Zhu, H. Zhang, *J. Mater. Chem. C* **6**, 9582 (2018)
36. J.R. Brent, D.J. Lewis, T. Lorenz, E.A. Lewis, N. Savjani, S.J. Haigh, G. Seifert, B. Derby, P. O'Brien, *J. Am. Chem. Soc.* **137**, 12689 (2015)

Publisher's Note Springer Nature remains neutral with regard to jurisdictional claims in published maps and institutional affiliations.